J. Fluid Mech. (2015), *vol.* 779, *pp.* 751–775.
doi:10.1017/jfm.2015.453

An experimental investigation of resonant interaction of a rectangular jet with a flat plate

K. B. M. Q. Zaman[1,†], A. F. Fagan[2], J. E. Bridges[3] and C. A. Brown[3]

[1]Inlets and Nozzles Branch, Propulsion Division, NASA Glenn Research Center, Cleveland, OH 44135, USA

[2]Optics and Photonics Branch, Communication and Intelligent Systems Division, NASA Glenn Research Center, Cleveland, OH 44135, USA

[3]Acoustics Branch, Propulsion Division, NASA Glenn Research Center, Cleveland, OH 44135, USA

(Received 2 October 2014; revised 12 June 2015; accepted 30 July 2015; first published online 21 August 2015)

The interaction between an 8:1 aspect ratio rectangular jet and a flat plate, placed parallel to the jet, is addressed in this study. At high subsonic conditions and for certain relative locations of the plate, a resonance takes place with accompanying audible tones. Even when the tone is not audible the sound pressure level spectra are often marked by conspicuous peaks. The frequencies of these peaks, as functions of the plate's length, its location relative to the jet as well as jet Mach number, are studied in an effort to understand the flow mechanism. It is demonstrated that the tones are not due to a simple feedback between the nozzle exit and the plate's trailing edge; the leading edge also comes into play in determining the frequency. With parametric variation, it is found that there is an order in the most energetic spectral peaks; their frequencies cluster in distinct bands. The lowest frequency band is explained by an acoustic feedback involving diffraction at the plate's leading edge. Under the resonant condition, a periodic flapping motion of the jet column is seen when viewed in a direction parallel to the plate. Phase-averaged Mach number data on a cross-stream plane near the plate's trailing edge illustrate that the jet cross-section goes through large contortions within the period of the tone. Farther downstream a clear 'axis switching' takes place for the time-averaged cross-section of the jet that does not occur otherwise for a non-resonant condition.

Key words: aeroacoustics, jet noise, flow–structure interactions

1. Introduction

Driven by noise reduction goals, some newer aircraft concepts involve over-the-wing engine designs which might provide a shielding effect for the jet noise propagated towards the ground. Such a configuration is also desirable for sonic boom reduction with supersonic vehicles since the shock waves from the engine components would be directed upwards rather than towards the ground. In these concepts rectangular geometries for the jet nozzle are preferred for ease of integration with the airframe and also for possible noise benefits that might be inherent to the non-axisymmetric

† Email address for correspondence: khairul.b.zaman@nasa.gov

geometry (Balsa *et al.* 1978; Von Glahn 1989; Massey, Ahuja & Gaeta 2004; Nichols *et al.* 2011). However, with such concepts the flow just downstream of the nozzle is close to a surface before emanating as a free jet and jet–surface interaction becomes an important issue. In 2012 a research effort was initiated to investigate this experimentally. Plans were developed for detailed experiments in the Aeroacoustics Propulsion Laboratory (AAPL) of NASA Glenn Research Center (GRC). In support of these plans, and in order to provide a database for an ongoing analytical effort in a timely manner, it was decided that a preliminary experiment be carried out in a relatively smaller facility during the autumn of 2012. Hot-wire surveys at low Mach numbers and Pitot-probe surveys at high Mach numbers together with limited noise measurements for both the 'reflected' and 'shielded' sides of the plate were conducted. A comparison of the results with an analysis was made by Afsar, Goldstein & Leib (2013); see also Goldstein, Afsar & Leib (2013) for details of the analysis.

During the course of the latter experiments in the smaller facility, an unexpected resonant interaction was encountered. It occurred for certain ranges of the plate's location relative to the nozzle and at high subsonic Mach numbers. It was accompanied by audible tones that obviously had an impact on the radiated noise. It also had an impact on the flow field in a profound manner in that the jet cross-section went through an 'axis switching' that did not occur otherwise in the absence of the tone. There is a body of literature on past experimental studies of trailing-edge noise and jet–wing and jet–flap interaction noise (e.g. Tam & Yu 1975; Yu & Tam 1978; Olsen & Boldman 1979; Way & Turner 1980; Miller 1983; SenGupta 1983; Brown & Ahuja 1984; Mead & Strange 1998; Mengle 2011). For a review of past analytical as well as experimental efforts in these areas an interested reader may refer to Crighton (1991). However, a resonance-like behaviour involving the emission of sharp tones was seldom reported, to the best of the authors' knowledge. An understanding of the resonant interaction is important not only to guide future research in the area but also so that it could be avoided or suppressed in possible applications. Note that the issue may be pertinent to both over- and under-the-wing engine configurations.

While pertinent past observations on jet–surface interaction will be discussed in the results section, here a brief overview of aeroacoustic resonance phenomena akin to the one in hand may be worthwhile. An account of sustained oscillations with impinging jets can be found in the paper by Rockwell & Naudascher (1979). The phenomenon of 'edgetone' occurs when an 'edge' or a wedge is placed in the middle of a jet (Powell 1961). Instability waves grow in the jet's shear layer to form vortices which upon impacting the wedge produce pressure pulses. The pressure pulses propagate upstream and interact with the nozzle lip to introduce new instability waves in the shear layer. The feedback loop is thus completed, sustaining the resonance with the emission of a sharp tone. A similar mechanism is in play with the 'screech' phenomenon involving imperfectly expanded supersonic jets. Here the vortices interact with a standing shock cell structure, rather than with a wedge, to set up the feedback loop (see e.g. Powell 1953; Tam 1995). Another class of flows, having similarity with the phenomenon under study, involves jets discharging through ducts or ejectors (e.g. Nomoto & Culick 1982; Samanta & Freund 2008; Zaman, Clem & Fagan 2013). A feedback loop may be set up between the jet nozzle and a section of the duct involving sudden area change. However, here the acoustic resonance modes of the duct can couple to render the tones very loud. In engine test facilities this sometimes creates a 'howl' that apart from the noise issue may raise serious structural concerns (Jones & Lazalier 1992). For the phenomenon under study, as elaborated later, preliminary experiments convinced us that a simple edgetone-like

feedback between the plate's trailing edge and the jet nozzle was insufficient to explain the frequencies. It was decided that a detailed exploration of the phenomenon was worthwhile for, apart from academic curiosity, its possible relevance to practical applications.

Thus, while detailed experiments on jet–surface interaction simulating realistic flight situations were conducted in the AAPL (Bridges, Brown & Bozak 2014; Brown & Wernet 2014), the resonance phenomenon was pursued further in the smaller facility. The latter study involved the simple geometry of a rectangular flat plate of large width placed on one side of the jet. An 8:1 aspect ratio rectangular nozzle was used and the plate was placed parallel to the major-axis plane. Parametric dependence of the resonance was explored by varying the jet Mach number, streamwise length of the plate as well as the plate's transverse and axial locations. Preliminary results of the study have been presented earlier (Zaman *et al.* 2014). This paper summarizes those earlier results and presents further results from later explorations. The experimental procedures are described first, followed by a discussion of key results and concluding remarks.

2. Experimental facility and procedure

An open jet facility, referred to as 'CW17', at NASA GRC was used for the study. Compressed air passed through a 76 cm diameter plenum chamber before exhausting through the nozzle into the ambient of the test chamber. Only cold (unheated) flows were considered; an interested reader may find further description of the facility in earlier papers, e.g. Zaman (2012). With a suitable adapter, the same nozzles used in the AAPL could be investigated in this facility and vice versa. The 8:1 aspect ratio nozzle, referred to as 'NA8Z' by Frate & Bridges (2011) and simply as 'R8' herein, was used in the experiment. It was one of the nozzles that in combination with different surfaces were to be studied in the AAPL experimental program. The design considerations for a class of rectangular nozzles including the R8 have been discussed by Frate & Bridges (2011). Detailed coordinates of the nozzle, suitable for adaptation in numerical simulation, can also be found in Zaman (2012). The nozzle exit had dimensions of 13.56 cm $\times$ 1.67 cm and thus an equivalent diameter $D = 5.39$ cm. Because plates with different lengths have been used and since there is some ambiguity regarding whether the equivalent diameter or the long or the short dimension of the nozzle is the appropriate length scale, the results are presented simply in dimensional form with unit of distance in cm. Furthermore, when quoting a dimension in equation form, the notation 'cm' is dropped for brevity.

The experiment was started with a 1.27 cm thick and 61 cm wide aluminium plate that was 30.5 cm long in the streamwise direction. The trailing edge (TE) of the plate had a 45° bevel while the leading edge (LE) was square. (The 45° single bevel angled backwards from the top so that the flow exited a sharp edge.) By reversing the plate's orientation it was determined that the bevelled or the square shape of the trailing edge produced the same resonance with practically identical noise spectra. Thus, a square shape was chosen for both LE and TE for all subsequent experiments, which allowed procurement of the plates from stock without requiring significant machining. Figure 1(*a*) is a photograph of the overall setup for the experiment; a schematic with coordinate system is shown in figure 1(*b*). Plates of varying streamwise lengths, $L = 5.08$, 10.16, 20.32, 30.48 and 40.64 cm, were used. These will be denoted in the following as '*L*5', '*L*10', '*L*20', '*L*30' and '*L*40', respectively, for brevity. All plates were 1.27 cm thick and 61 cm in width. In some experiments, combinations

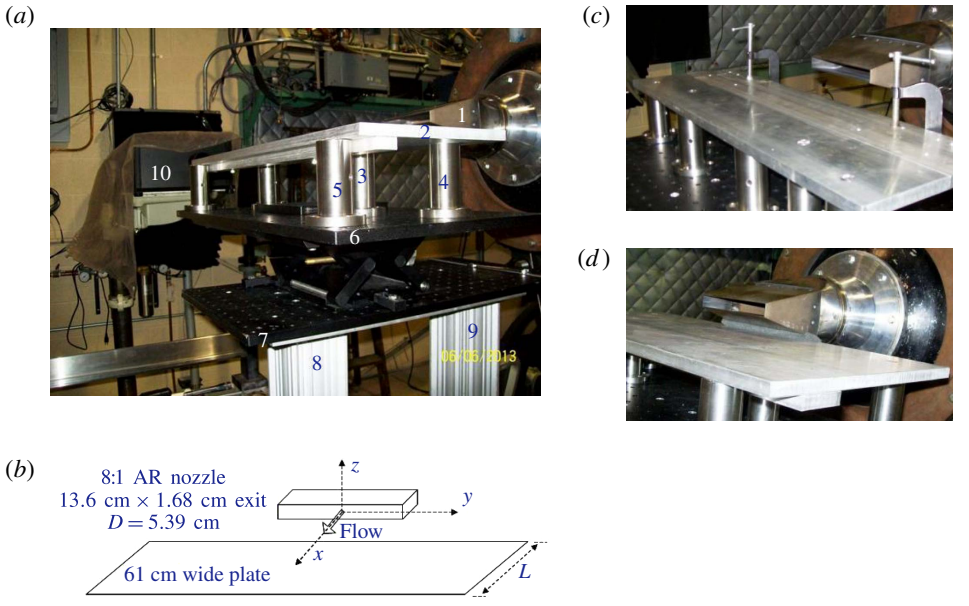

FIGURE 1. (Colour online) Experimental facility. (*a*) Setup with marked components. 1: nozzle; 2: plate; 3–5: mounting posts; 6, 7: breadboards; 8, 9: supports; 10: focused schlieren apparatus. (*b*) Schematic of setup with coordinates. (*c*) Extender bars added to a plate. (*d*) Setup to explore feedback path.

of $L = 1.27$, 2.54, 3.81 cm bars, with same thickness and width as the plates, were used together with the plates to vary the total length L in increments of 1.27 cm. Figure 1(*c*) shows a picture of an arrangement for adding the bars. Care was taken to keep the upper surface smooth and the data were compared with single-plate data, whenever possible, to make sure that the addition of the rails underneath or the c-clamps did not alter the noise spectra. Figure 1(*d*) shows an arrangement where sound absorbing foam material was wedged in the gap between the plate's leading edge and the underside of the nozzle; the purpose will be described later in the text. It should be noted that all noise spectra data were obtained after wrapping the face of the plenum chamber with sound absorbing material. However, tests with and without the wrapping material showed no perceptible difference in the spectra when a resonance occurred.

For all data, the plate was placed aligned with the nozzle's long edge, centred in the lateral (y) direction relative to the jet axis, and parallel to the x–y plane. The transverse (z) location of the plate could be varied manually using a heavy duty 'lab-jack' (located between the breadboards marked 6 and 7 in figure 1*a*). The axial (x) location could also be varied manually in coarse steps by sliding the plate assembly on breadboard 7. At the start of the experiment, attempts were made to mount the assembly on a traversing mechanism so that the surveys could be done under automated computer control. However, the idea had to be abandoned due to structural vibration concerns, an issue discussed further in the results section.

The test cell had acoustic linings on the ceiling and upper walls and with proper preparation measurement of the radiated noise was possible. The semi-anechoic condition did not permit accurate measurement of the amplitudes; however, relative amplitudes with parametric variation were well represented. The quality of the noise

data has been discussed in prior publications of the first author (an interested reader may refer to Zaman 2012). For the present study, the precise amplitudes of the sound pressure level (SPL) spectra are of little concern since the study focuses mainly on the parametric dependence of the resonant tone and its frequency. Microphones (0.635 cm, B&K 4135) held fixed on an overhead arm at polar locations $\theta = 25°$, 60°, 75° and 90° were used for the noise measurements; θ is referenced with respect to the jet's downstream axis. For brevity, most of the noise data presented in the following pertain to $\theta = 60°$. As discussed later, surveys showed that the tone was detected most prominently around this location. The 60° microphone was 127 cm from the centre of the nozzle's exit. Spectral analysis was done over 0–10 kHz with a bandwidth of 12.5 Hz. The bandwidth primarily dictated the uncertainty in the measurement of the tone frequency.

A focusing schlieren system was used for flow visualization The system is based on a lens-and-grid technique where a source grid is projected onto a retro-reflective screen and imaged onto a cut-off grid creating the schlieren effect; an interested reader may find details and further references in Fagan, L'Esperance & Zaman (2014). The light source illuminating the flow field had 1 μs pulse duration. All optical components, as well as the scientific-grade charge coupled device (CCD) camera, were housed in a 58 cm × 43 cm × 25 cm case (item 10 in figure 1*a*). The case was placed on one side of the jet while the 76 cm × 61 cm retro-reflective screen was placed on the other side. The distances of the two items from the jet's centreplane dictated the size of the field of view. The chosen distances, within the constraints of the test chamber, provided a field of view that extended approximately 23 cm in the streamwise direction. The thickness of the focused field (in the y-direction) was about 7.6 cm. The pictures shown in the following are essentially instantaneous snapshots of the flow field capturing the unsteady vortical structures and the shocks when present.

Steady-state flow field surveys were done with a rake of three Pitot probes. The spacing of the probes in y was 1.22 cm and this was the spatial resolution in that direction for those measurements. Mean Mach number data were acquired over the cross-sectional (y–z) plane and the data were normalized by the jet Mach number, Ma_j, as defined below. During the surveys, even though the plenum pressure was held by automated feedback control, fluctuations occurred depending on other facilities using the 'central air supply'. This contributed to the largest uncertainty in the plenum pressure. However, the Mach number data were normalized by the 'current' jet Mach number (Ma_j) calculated from the plenum pressure (p_0) read simultaneously with the Pitot data. The root-mean-square (r.m.s.) fluctuation in Ma_j (in percent of average Ma_j), calculated over an entire run, was less than 0.5 % for all data shown. The jet Mach number was calculated from the plenum pressure (p_0) and the ambient pressure (p_a) via the isentropic relation, $Ma_j = (((p_0/p_a)^{(\gamma-1)/\gamma} - 1)(2/(\gamma - 1)))^{1/2}$, γ being the ratio of specific heats for air. The experiments were conducted at jet Mach numbers ranging from 0.5 to about 1.06; the maximum Reynolds number based on D was about 1.73×10^6.

The unsteady flow field surveys were done with a miniature pressure transducer (Endevco 8507c-15). It was mounted at the end of a 23 cm long support that telescoped from a root diameter of 0.635 cm to a sensor diameter of 0.16 cm. It was inserted straight into the flow, similarly to a Pitot probe. The probe essentially responded to unsteady total pressure. During the process of mounting the probe with the telescoping tubes the calibration changed somewhat from the manufacturer's specification. Estimated calibration (using a piston phone with 124 dB limit) was applied and the amplitudes of the unsteady flow data should be considered qualitative.

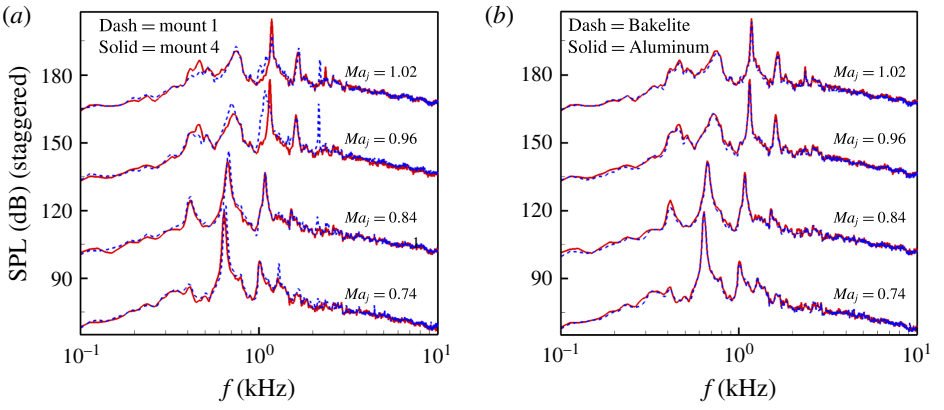

FIGURE 2. (Colour online) SPL spectra for plate $L20$ ($L = 20.32$ cm) at four jet Mach numbers (Ma_j): (a) for different rigidity of plate mounting structure, (b) for plates of different material. Pairs of traces are staggered successively by 15 dB, ordinate pertains to the pair at the bottom.

3. Results

3.1. *Ruling out structural vibration effect*

At the start of this investigation structural vibrations were encountered affecting the noise spectra. Such effects were suspected when the frequency of a spectral peak would not change upon variation of Ma_j, and confirmed when the amplitude of the spectral peak changed upon addition of stiffeners to the plate assembly. It was imperative to suppress these effects, first in order to confirm that the resonant tones were not due to structural vibration and then to enable a study of their fluid dynamic characteristics. The approach taken to resolve this issue was to progressively add stiffeners to the plate and its mounting structure until the noise spectra did not change any more.

At first, the $L30$ plate ($L = 30.48$ cm, see § 2) was mounted on a pair of posts placed symmetrically on its major axis. This pair, marked '3' in figure 1(a), can be seen underneath the plate between two other pairs, marked 4 and 5. (In each pair the nearer post is marked and the two in a given pair are placed symmetrically about the x–z plane.) Pairs 4 and 5 were added later as described in the following. The plate was firmly bolted to the 3.81 cm diameter posts of pair 3 and thought to be rigid enough for the experiment. However, a peak around 500 Hz appeared consistently in the noise spectra. This appeared to be the same frequency as that at which the plate would 'sing' upon an impact. It was estimated to be the first flexural mode about the major axis. There were also other peaks in the spectra suspected to be related to structural vibration.

At this point the pair of posts marked 4 was added. The noise spectra were checked as the structural changes were made in steps. Supports marked 8 and 9 were then firmly anchored to the vibration-isolated floor of the test chamber. This configuration, referred to as 'mount 1', took out most of the suspicious spectral peaks. These tests were done with the $L30$ as well as the $L20$ plate. Figure 2(a) shows pairs of SPL spectra taken at four jet Mach numbers for the $L20$ case. Comparison is made between 'mount 1' and the final configuration ('mount 4') that included another pair of posts (marked '5' in figure 1a) together with additional stiffeners on the under

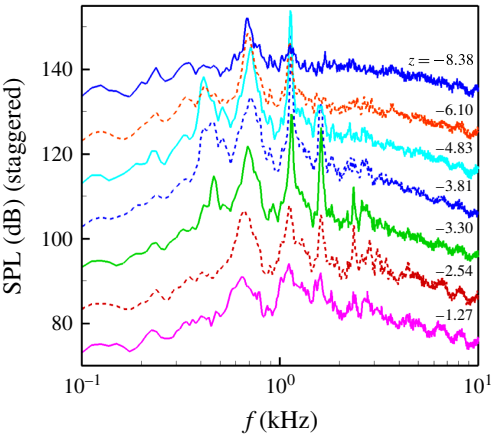

FIGURE 3. (Colour online) SPL spectra for varying z-location (in cm) of plate $L20$; $x_{TE} = 21.6$, $Ma_j = 0.96$.

sides of the plate as well as both breadboards 6 and 7. 'Mount 1' still involved some structural modes as evident from the spectral peak around 2150 Hz, especially visible at higher values of Ma_j. This went away when the stiffeners were added. These additions were made to the support mechanism in steps (from 'mount 2', to '3', to '4') until the spectra did not change any more. As a final proof another set of data was taken by replacing the $L20$ aluminium plate with a plate of the same dimensions but made of a different material (Bakelite). Figure 2(*b*) shows spectral pairs for the two plates at four values of Ma_j. If any of the spectral peaks were due to a certain structural mode the frequency would decrease substantially with the Bakelite plate (by a factor of 2 from rough estimates). The four pairs of spectra are virtually identical, providing confidence that the observed peaks must be fluid dynamic in origin. (While the data compared in figure 2(*a*,*b*) were obtained in back-to-back experiments, after major changes in the setup and reinstallation, the relative amplitudes of the spectral peaks were noted to vary somewhat. This was likely to be due to slight differences in the exact configuration.)

3.2. *Parametric dependence*

Parametric dependence of the resonance was explored. Even though detailed data were taken with various plates, only sample results highlighting the key observations are presented in the following. Figure 3 shows SPL spectra for varying z-location of plate $L20$ in a 'waterfall' pattern. The traces are staggered by one ordinate division with the scale pertaining to the trace at the bottom. The axial location of the plate's trailing edge and leading edge were held at $x_{TE} = 21.6$ and $x_{LE} = 1.27$, respectively. The z-location (in cm) for each spectral trace is indicated in the figure. Each spectral trace is characterized by multiple peaks. A peak at about 1200 Hz becomes dominant around $z = -3.81$. This is accompanied by a clearly audible tone (audible to bare ears from the control room of the test chamber). With varying z-location, the frequency of the tone varies slightly; however, the amplitude changes significantly. The amplitude variations with z for four different plates, all with $x_{TE} = 21.6$, are shown in figure 4. Overall sound pressure level (OASPL) data are shown. OASPL is dominated by

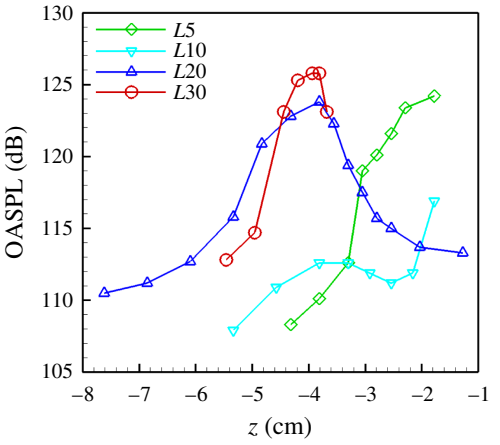

FIGURE 4. (Colour online) Overall sound pressure level for varying z-location of different plates; $x_{TE} = 21.6$, $Ma_j = 0.96$.

the tone when it is strong and, therefore, was enough to provide an idea about the intensity of the resonance. For plates $L30$ and $L20$, it is apparent that the amplitude is large within a range of z. The tone occurs within that range and disappears when the plate is either too close to or too far from the jet. (Note that with the given x_{TE} the leading edge of plate $L30$ touched the under surface of the nozzle when $z = -3.57$, and thus it could not be moved any closer to the jet.) For the $L10$ case, there is a similar trend; however, for both $L10$ and $L5$ cases other noise components come into play when they are placed too close to the jet, possibly due to the impact of the flow also on the LE.

Sample schlieren flow visualization images are shown in figure 5 for plate $L20$. The data pertain to $x_{TE} = 21.6$ for four z-locations of the plate with $Ma_j = 0.96$. As stated before, the pictures represent 'instantaneous' snapshots with 1 μs exposure time. For $z = -1.27$ and -2.54 (plate close to the jet in (a) and (b)) the resonant tone is either absent or weak (see amplitude data in figure 4) and the jet basically hugs the plate surface. At $z = -3.43$, however, there is a clear tone at 1190 Hz and this is accompanied by an undulating flapping motion of the jet column (figure 5c). A rolled-up vortical structure is apparent just past the trailing edge. For $z = -5.59$, on the other hand, the tone has ceased and the path of the jet has become relatively straight (figure 5d).

Another set of schlieren data is shown in figure 6 illustrating the effect of jet Mach number. Data for four values of Ma_j are shown for the $L30$ plate with $x_{TE} = 21.6$, $z = -3.81$. At the lowest Ma_j of 0.76 (figure 6a) there is no audible tone and the path of the jet is straight. When the tone occurs, at $Ma_j = 0.86$ in figure 6(b) or $Ma_j = 0.99$ in figure 6(c), it is evident that the jet goes through a flapping motion similar to that seen in figure 5(c). (SPL spectra with variation of Ma_j are shown later.) At $Ma_j = 1.06$ (figure 6d), on the other hand, the tone has ceased and the path of the jet has become straight. A shock structure in the jet plume has also appeared at the latter Ma_j.

Before proceeding with data on detailed parametric variation, the 'directivity' of the noise may be examined from the spectra data shown in figure 7. SPL spectra for all four measurement locations exhibit similar peaks at identical frequencies. The resonance is likely to involve a feedback mechanism, as discussed later, and involves

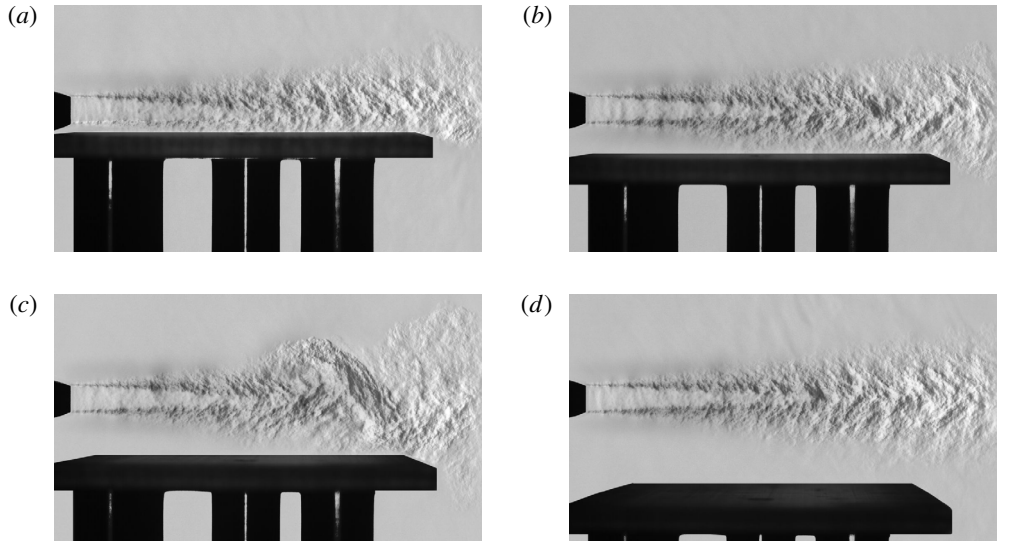

FIGURE 5. Schlieren images of flow field for varying z-location of plate $L20$; $x_{TE} = 21.6$, $Ma_j = 0.96$. (*a*) $z = -1.27$, (*b*) $z = -2.54$, (*c*) $z = -3.43$ and (*d*) $z = -5.59$.

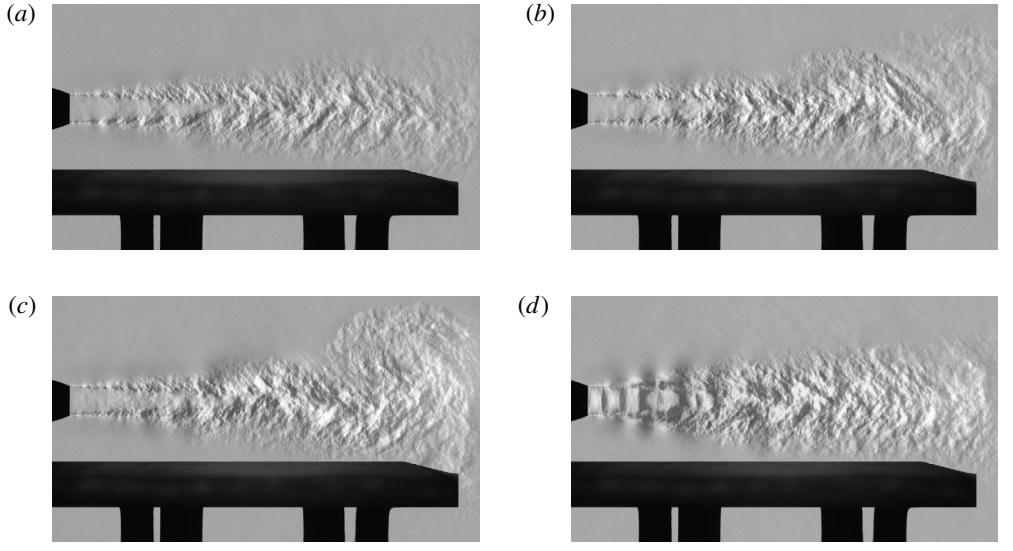

FIGURE 6. Schlieren images of flow field for plate $L30$ at four Ma_j; $x_{TE} = 21.6$, $z = -3.81$. (*a*) $Ma_j = 0.76$, (*b*) $Ma_j = 0.86$, (*c*) $Ma_j = 0.99$ and (*d*) $Ma_j = 1.06$.

sharp peak(s). These are heard everywhere and the frequencies can be measured from any of the spectra. It is also noted that the tone amplitude is larger in the upstream direction (similar to the screech phenomenon with imperfectly expanded jets). Data for several cases indicate that the tone is heard the loudest around $\theta = 60°$. In this paper, we concern ourselves with the mechanism of frequency selection for the tone(s) and hence for brevity all subsequent data are presented only for the $\theta = 60°$ location.

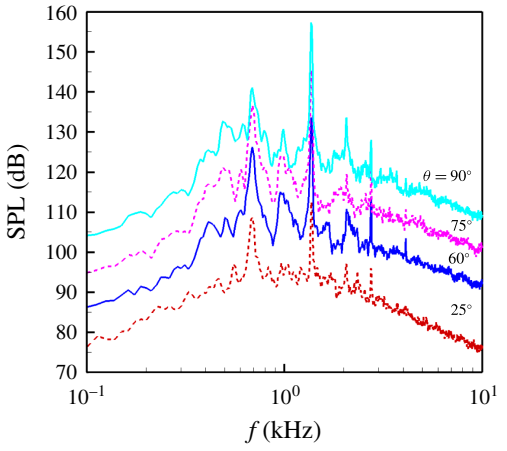

FIGURE 7. (Colour online) SPL spectra for plate $L30$ with $x_{TE} = 21.6$ and $z = -3.89$; $Ma_j = 0.96$. Data are for all four polar locations, as indicated; successive curves are staggered by 10 dB for easy identification.

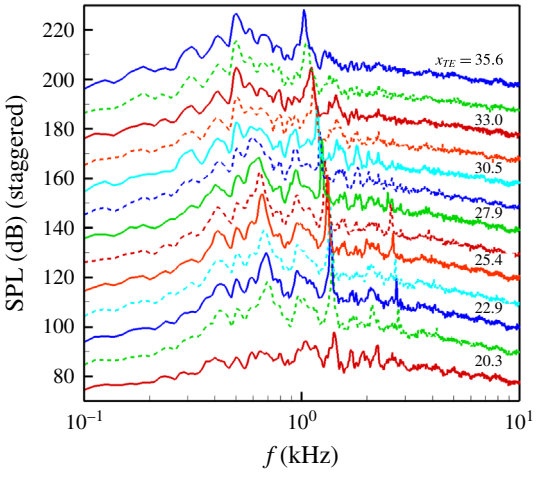

FIGURE 8. (Colour online) SPL spectra for plate $L30$ with varying x_{TE}; $Ma_j = 0.96$. Plate z-location varied approximately as $z = 1.37 + 0.12x_{TE}$. Ordinate pertains to the trace at the bottom, others staggered successively by 10 dB. Successive traces are for 1.27 cm increment in x_{TE}.

Detailed spectral data for parametric variation were obtained. Data for the $L30$ plate, with increments of 1.27 cm in trailing edge location x_{TE}, are shown in figure 8. The values of x_{TE} are indicated for alternate traces; the z-location is changed as indicated in the figure caption in order to produce the resonance with approximately the maximum amplitude. (The equation for z quoted in the figure caption was fitted after the experiment. Since each change in z had to be done manually by shutting down the flow, the changes were done in coarse steps. The values are within ± 0.25 cm of the prediction from the equation.) With increasing distance a sharp spike around 1400 Hz ensues at $x_{TE} = 21.6$. The frequency of the tone decreases monotonically with further increase in x_{TE}. Note that in each spectrum, besides the dominant peak

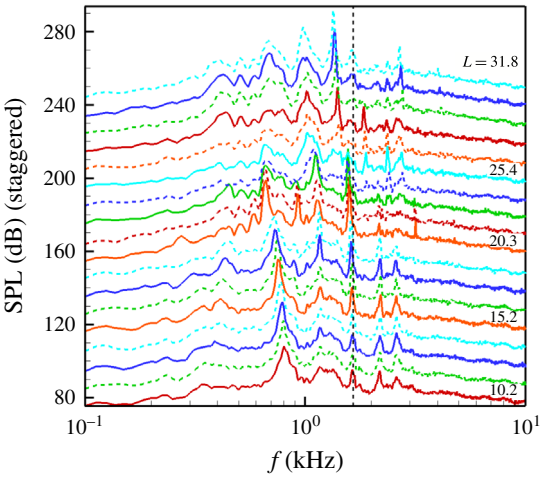

FIGURE 9. (Colour online) SPL spectra for fixed TE location of plate ($x_{TE} = 21.6$ and $z = -3.94$) but varying L (hence varying LE location, x_{LE}); $Ma_j = 0.96$. Traces are staggered and successive traces are for 1.27 cm increment in L.

there are other conspicuous peaks. The characteristics of these spectral peaks and the variation of their frequencies with x_{TE} are analyzed and discussed in the following.

From figures 5–8, one might get the impression that the phenomenon under consideration might be akin to the classical edgetone phenomenon (Brown 1937; Powell 1961). Here, the resonance might be occurring due to sound pulses produced during the passage of the vortices over the plate's trailing edge. The sound pulses travel back to the nozzle lip to produce nascent vortices completing the feedback loop. This notion, however, conflicts with the following data. Figure 9 shows spectral data where the trailing edge of the plate is held fixed ($x_{TE} = 21.6$, $z = -3.94$) while the length L is varied in increments of 1.27 cm. If the resonance were due simply to a feedback between the plate's TE and the nozzle exit, one might expect the resonant frequency to remain unchanged. An inspection of figure 9 should convince one that this is not the case. Even though some of the spectral peaks appear to remain unchanged for smaller values of L there are significant changes at larger L; a vertical dashed line is drawn at 1.64 kHz to make this clear. (The experiment was started with plates of fixed lengths. For $L = 15.2$, 20.3 and 30.5 cm the frequencies of the main peak around the dashed line were 1.64, 1.58 and 1.36 kHz, respectively. This was the anomaly that confronted us at the beginning of the investigation. Only after varying L systematically do the underlying trends became clear.) The frequency variations are further discussed shortly.

It is apparent that the leading edge location also comes into play in determining the various spectral peaks. This is further examined in figure 10 where the leading edge is held fixed ($x_{LE} = 0$, $z = -4.57$) while L is varied, again in increments of 1.27 cm. Large changes in the spectral shape also take place with variation of L. Thus, LE location alone also does not determine the frequency.

While the data shown in figures 7–10 pertain to a fixed jet Mach number $Ma_j = 0.96$, the effect of Ma_j for the $L30$ plate with fixed position is shown in figure 11. One finds that a sharp spike accompanied by an audible tone ensues with increasing Mach

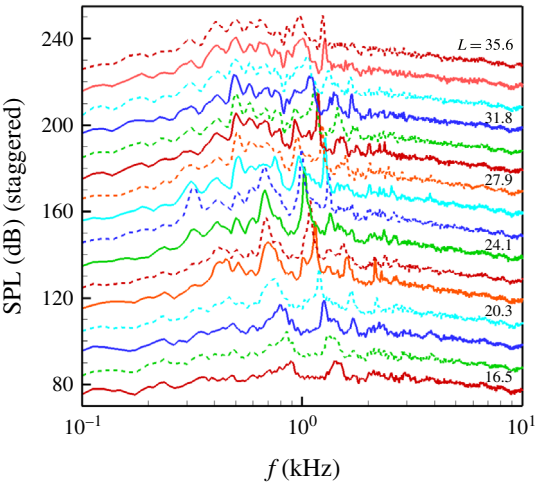

FIGURE 10. (Colour online) SPL spectra for fixed LE location of plate ($x_{LE} = 0$, $z = -4.57$) but varying L (hence varying x_{TE}); $Ma_j = 0.96$. Traces are staggered and successive traces are for 1.27 cm increment in L.

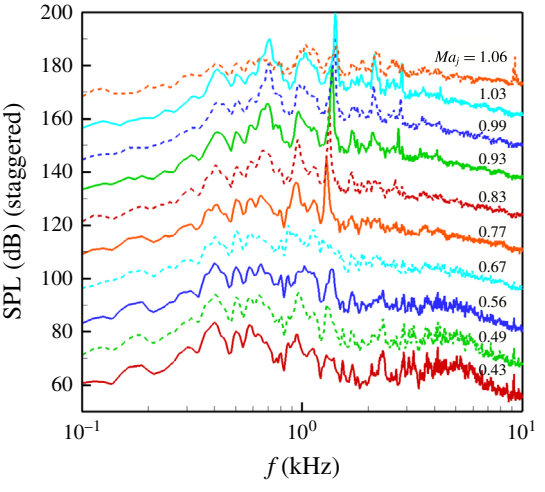

FIGURE 11. (Colour online) SPL spectra for varying Ma_j with plate $L30$; $x_{TE} = 21.6$, $z = -3.81$. Traces are staggered in the same manner as in previous figures.

number from around $Ma_j = 0.77$, for the given configuration. The resonance persists throughout the transonic regime but abruptly stops around $Ma_j = 1.06$; see schlieren images in figure 6.

The spectral data are now analyzed as follows. Each spectrum is scanned for the highest three peaks. Even though in some cases the smaller peaks may be at the noise level, a look at the characteristics of these peaks reveals some orderly trends. First, for a clarification of the method, the amplitudes of the peaks for the case corresponding to figure 9, are shown in figure 12. The circular, diamond and triangular symbols represent the spectral peaks in order of diminishing amplitudes. OASPL values are also shown in the figure by the square (solid) symbols. The

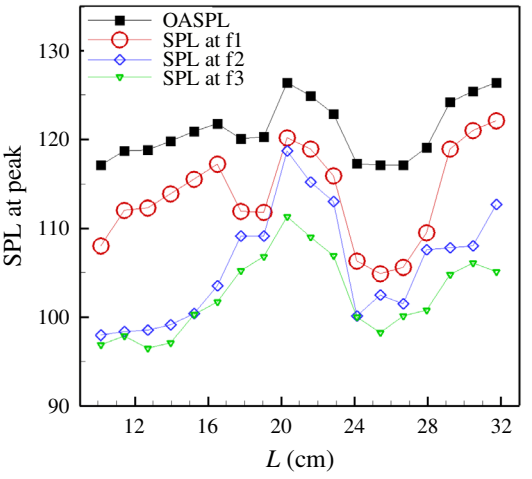

FIGURE 12. (Colour online) Amplitudes of the three highest peaks in the spectra of figure 9; varying L with fixed $x_{TE} = 21.6$, $z = -3.94$; $Ma_j = 0.96$.

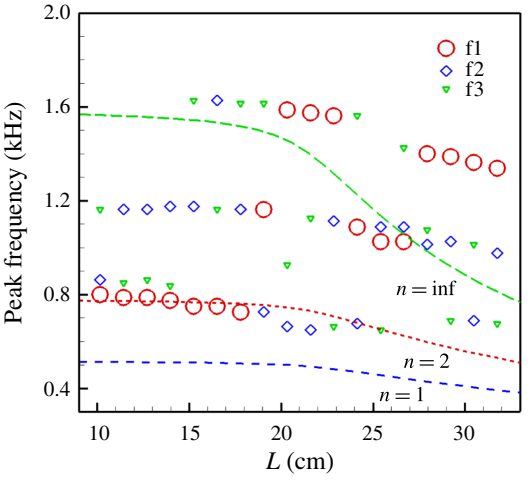

FIGURE 13. (Colour online) Frequencies of the three highest peaks in the spectra of figure 9. Varying L with fixed $x_{TE} = 21.6$, $z = -3.94$; $Ma_j = 0.96$. f1, f2 and f3 denote three peaks in order of deceasing amplitude. Lines for equation (3.1) (see text).

undulations in the amplitudes of the largest peak (circular symbols) are apparently due to a 'staging' behaviour, as will become clear with the frequency data shown next.

Variations in the frequencies of the three highest spectral peaks, corresponding to the case of figures 9 and 12 (fixed TE, varying L), are shown in figure 13. At small values of L, the highest peak occurs around 800 Hz. The frequency decreases with increasing L until at around $L = 17.8$ the highest peak shifts to a higher frequency band. With further increase in L, it shifts to a yet higher frequency, followed by some oscillations between the upper two bands. Overall, there appear to be three frequency bands starting at approximately 800, 1200 and 1600 Hz, for the case

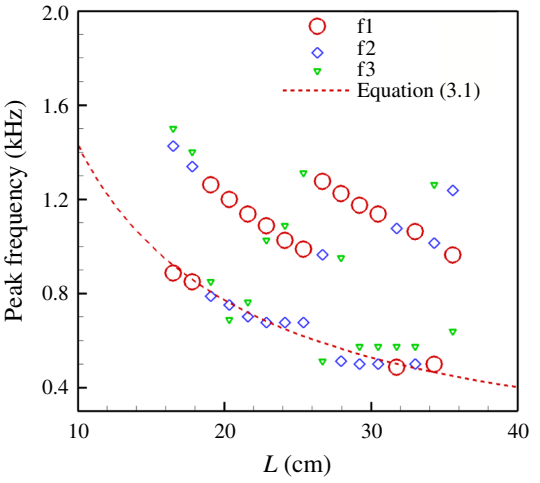

FIGURE 14. (Colour online) Frequencies of the three highest peaks in the spectra of figure 10; fixed LE of plate ($x_{LE} = 0$ and $z = -4.57$) but varying L (hence varying x_{TE}).

under consideration. Ignoring some data scatter, it is clear that there is an underlying pattern and all frequency data fall in these distinct bands. Peaks representing each band are always there in the spectra and one of them becomes dominant depending on geometric configuration. It is noted that generally the frequencies of the three peaks are not multiples or submultiples of one another. On occasions, they seem to be multiples but this could be a coincidence. Also shown in figure 13 are curves denoted 'Equation (3.1)' that will be described shortly.

Similar frequency variations for the three highest spectral peaks corresponding to the data of figure 10 (fixed LE, varying L) are shown in figure 14. A similar observation can be made as for figure 13. Again, the frequency data are not random and fall in one of the multiple bands. The same appears true for jet Mach number variation with a fixed plate, as seen from the frequency data in figure 15 corresponding to the spectral traces of figure 11. Referring back to figure 8 (varying x_{TE} with fixed L), a similar analysis yields the frequency data shown in figure 16. The frequencies of the highest peaks again cluster in certain bands. Finally, similar frequency data for the effect of z-variation with the $L20$ plate are shown in figure 17. These data correspond to the spectral data of figure 3. A similar observation can be made as for figures 13–16.

3.3. *Possible mechanism*

Possible aerodynamics and acoustic feedback involved in the phenomenon are considered with the sketches in figure 18. The fact that both the LE and TE of the plate influence the frequency of the spectral peaks led us to first consider the following feedback path. In figure 18(*a*), the likely distribution of the vortices is sketched. Inspection of the schlieren images (figures 5*c*, 6*b*,*c*) suggests that there may be multiple vortices over the length of the plate at a given instant. It appears that in most cases there are two vortices in the bottom shear layer over the length of the plate at a given instant. Let us assume that there are n such vortices. Each vortex produces a sound pressure pulse upon its passage past the TE. Let us also assume that the feedback takes place via a path underneath the plate. Then, using the notation in figure 18(*a*), the total period of the feedback process can be written

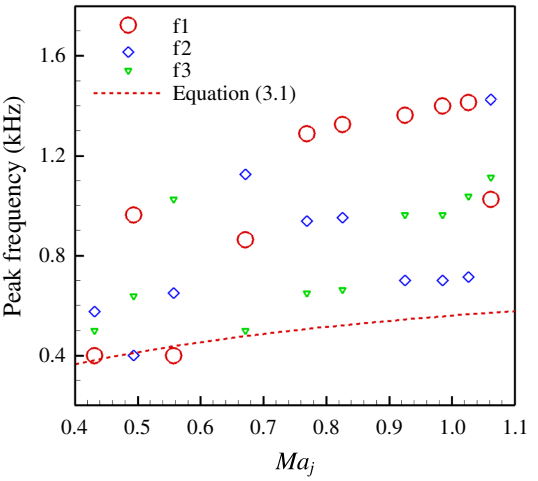

FIGURE 15. (Colour online) Frequencies of the three highest peaks in the spectra of figure 11; varying Ma_j for plate $L30$, $x_{TE} = 21.6$, $z = -3.81$.

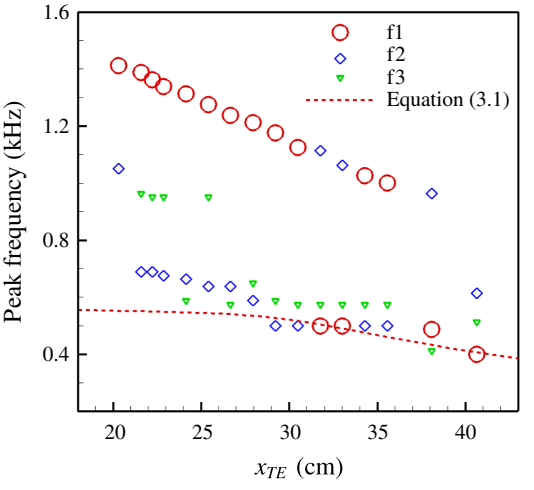

FIGURE 16. (Colour online) Frequencies of the three highest peaks in the spectra of figure 8; varying x_{TE} for plate $L30$.

as the sum of vortex passage time over the distance x_{TE}/n and the acoustic feedback time over the distance $L + s$. Assuming a vortex convection velocity equal to $0.5cMa_j$, where c is the speed of sound in the ambient, the following equation can be written for the frequency:

$$f = c/(2x_{TE}/nMa_j + L + s). \tag{3.1}$$

Note that the thickness of the plate has been neglected in determining the paths and also that $L = x_{TE} - x_{LE}$. The predictions from (3.1) have been shown in figures 13–17. In figure 13, predictions for $n = 1$, 2 and infinity are shown. To avoid clutter, the prediction only for $n = 2$ is shown in the subsequent figures. It is apparent that the prediction ($n = 2$) approximates the band of frequency data at the bottom of each figure. Before considering the sketch in figure 18(*b*) let us note the following. The fact

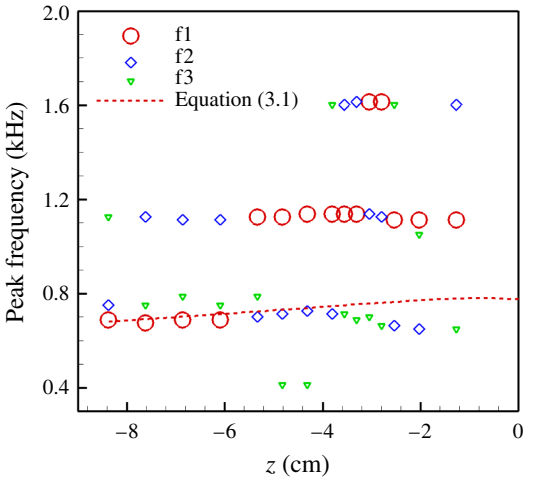

FIGURE 17. (Colour online) Frequencies of the three highest peaks in the spectra for varying z with plate $L20$; $x_{TE} = 21.6$, $Ma_j = 0.96$.

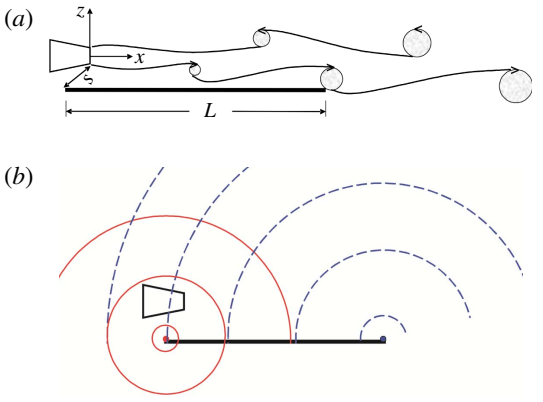

FIGURE 18. (Colour online) Schematics of flow and acoustic diffraction. (*a*) Likely distribution of vortices in the flow, (*b*) possible acoustic waves and diffraction from the LE.

that the path around the leading edge might be playing a role is further demonstrated by the following exercise. When a gap between the plate's LE and the underside of the nozzle (about 0.33 cm) is closed by sound absorbing foam material (figure 1*d*), the resonance is eliminated or weakened significantly. This is evident from spectral data shown in figure 19(*a*). With addition of the foam material the amplitudes of the spectral peaks get significantly reduced, from the dashed curve for the 'no foam' case to the solid curve for the 'foam' case.

It is clear that the feedback hypothesis considered above reasonably well explains the frequencies in the lowest band in all of figures 13–17. However, there were observations that conflicted with the assumed feedback via a path underneath the plate. It was found that if the gap between the underside of the nozzle and the plate's LE was closed by touching the two surfaces (without the sound absorbing material but leaving a hard junction) the spectral shape remained practically unchanged. This

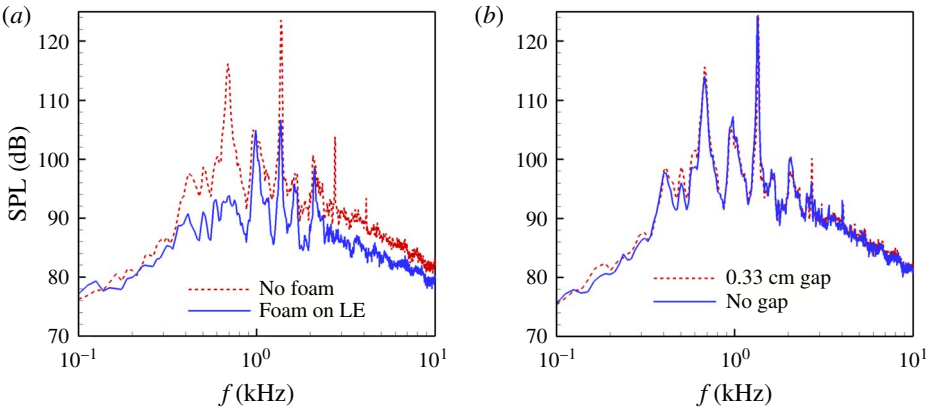

FIGURE 19. (Colour online) Effect of LE modification; plate $L30$, $x_{TE} = 21.6$, $Ma_j = 0.96$. (*a*) Effect of placing sound absorbing material near the LE (figure 1*d*), $z = -3.89$; (*b*) effect of closing the gap between the LE and the underside of the nozzle, $z = -3.56$.

is shown in figure 19(*b*). That is, a small gap or no gap made no difference in the spectra as long as the junction involved hard surfaces. Insertion of a metal strip in the gap (instead of the foam material) also made no difference in the spectra. However, as seen in figure 19(*a*), the peaks diminished significantly with the foam material. These observations suggested that the feedback may not be via a path under the plate and led to the following thought.

It is possible that diffraction from the LE creates a 'new' source of sound. This is schematically shown in figure 18(*b*). The sound originating from the TE, due to the passage of the vortices, may travel along a path over the surface (dashed wave fronts). The wave fronts are shown as if there were no flow to cause any distortion. They are also shown relatively packed for clarity (in reality they may be spaced wider, i.e. of longer wavelengths). The waves are diffracted at the LE whence new waves (solid fronts) are radiated in all directions. The new source due to diffraction at the LE is nearer to the nozzle lip and thus may have a stronger influence on the feedback in the following sense. The waves from the TE will also reach the nozzle lip but they have to travel through regions of flow and thus get distorted before impacting on the lip. The LE, on the other hand, is near the lip and in a region where there is no direct flow. Thus, the waves from the LE remain spatially coherent and undistorted when impacting on the nozzle lip. This might explain a stronger influence of the LE in the feedback process even though the original source of the sound waves is at the TE. The part of the dashed waves reaching the LE to get diffracted travels through regions where there is no significant flow (hugging the plate surface and partly through the boundary layer over the plate) and thus are not significantly distorted. With this scenario, it should be clear that the lengths of the feedback paths (TE to LE travelled by the dashed waves and LE to nozzle lip travelled by the solid waves, and passage over the distance x_{TE} by the vortices) remain the same as before, yielding the same equation (3.1) for the frequency. It is plausible that a sharp but hard junction near the leading edge, when the gap is closed, would also produce a similar sound source via diffraction, to that sketched in figure 18(*b*). It is not clear how much change one would expect in the latter source strength while going from a small gap to no gap. However, the radiation to the aft (towards the nozzle lip) must not have changed

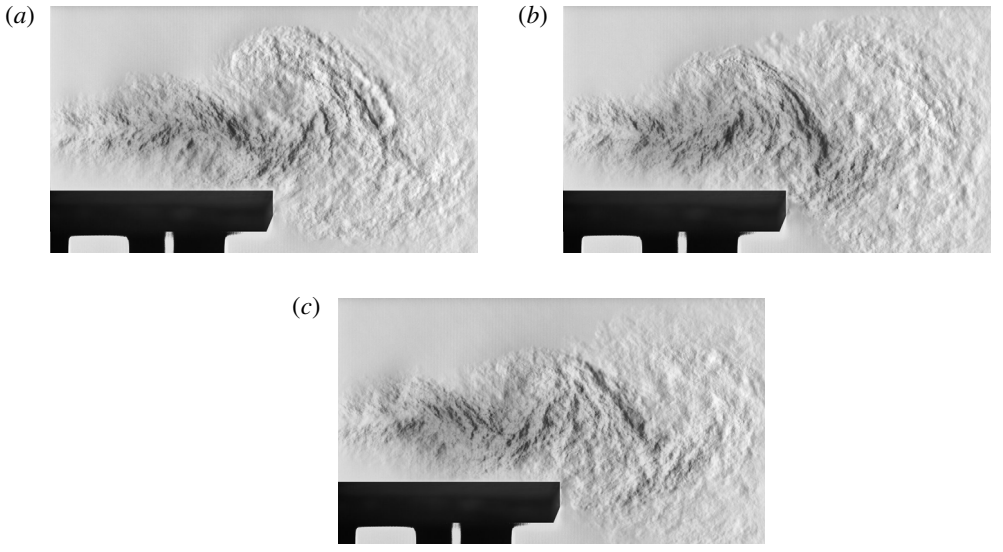

FIGURE 20. Focused schlieren images near the TE of plate $L30$; $Ma_j = 0.96$. Plate location ($x_{TE} = 21.6$, $z = -3.81$) yielded resonant tone at 1375 Hz. Unsteady flow pattern at three phases within a tone period: (*a*) $\varphi = 0°$, (*b*) $\varphi = 120°$ and (*c*) $\varphi = 240°$ (arbitrary reference for phase φ).

significantly since the two spectra in figure 19(*b*) are virtually identical. In summary it appears that the diffraction scenario provides a clearer rationale for (3.1).

A few earlier works on trailing-edge noise are worth noting here. Yu & Tam (1978) and Olsen & Boldman (1979) reported experimental results on the interaction of a rectangular (slot) jet with a flat plate. Both, however, involved wall jets (i.e. plate touching the lower lip of the nozzle), a configuration which did not produce a resonance in the present experiment. Yu & Tam presented shadowgraph data that exhibited large-scale turbulent motion similar to that seen in figure 5(*a*,*b*). Their data did not seem to exhibit the violent flapping motion seen in figures 5(*c*), 6(*c*) or figure 20 below. Their (averaged) spectral data were also smooth and did not display any peak. In an earlier paper, Tam & Yu (1975) also presented an analysis addressing sound generation by the interaction of the large-scale turbulent structures with the plate. Based on the analysis they noted, '... the noise directivity is strongly influenced by diffraction of sound at the leading edge of the plate'. For further comments on their analysis, as well as others, the reader may refer to Crighton (1991), but none of the analyses or experiments addressed a resonant condition and the associated frequencies. Olsen & Boldman (1979), on the other hand, presented narrow-band spectral data; some did exhibit sharp spikes that must have been associated with discrete tones. Unfortunately, the physical configuration of the plate relative to the flow was not completely clear. The plate used was large (several metres long by 2.43 m wide) but only 0.32 cm thick. We have seen how structural resonance can come into play and it remains unclear if the tones reported were due to structural modes or fluid dynamic in origin. A few other past works involving jet–airframe interaction noise are also pertinent. Miller (1983) presented experimental results and considered diffraction from the TE as well as the LE of the wing to explain spectral content and directivity of radiated noise. The data presented

by Mengle (2011), in connection with the effect of engine stand-off distance from the wing ('gulley height'), are worth noting. The noise spectra involved multiple peaks that were smeared due to the one-third-octave format of presentation but appeared to have similarity with some of the spectral shapes presented in this paper. Note that both of the latter references pertain to 'under-the-wing' engine configurations.

Referring back to the discussions of figures 13–17, it should be clear that (3.1) (with $n = 2$) predicts the 'fundamental' or the lowest band of frequencies for every parametric variation considered. However, not everything is explained and these weaknesses are discussed in the next paragraph. Here, it should be mentioned that various other possibilities were considered as possible mechanisms for the phenomenon. For example, vortex shedding from the entrained flow over the plate's leading edge was suspected as a source of unsteadiness. However, the exercise described with figure 19(*b*) ruled this out. Recall that by touching the LE with the under-surface of the nozzle the possibility of such vortex shedding was precluded, yet the resonant tone remained unaffected. Another possibility was considered based on interference of sound waves from the TE and LE (figure 18*b*). This could produce interference patterns and the feedback could be most effective when a high-amplitude 'crest' of the interference coincided with the nozzle lip. However, such an interference pattern may be complex and distorted since, as indicated before, the sound waves travel through regions of varying flow speed. Thus, the latter possibility also seemed unlikely.

The upper frequency bands in figures 13–17 may be considered as 'stages' and clearly strong resonance can also occur at those frequencies depending on parameters. In many resonance phenomena, e.g. edgetone or tones from impinging jets (Rockwell & Naudascher 1979), such a staging behaviour is observed. The various stages are harmonically related in the sense that, depending on the stage, a different but integral number of vortices occurs between the nozzle and the wedge (or ground in case of an impinging jet; the frequencies from one stage to another are often not exact multiples of each other). In the present case, if one assumes more than two vortices in the bottom shear layer ($n > 2$) the predicted frequency will be higher. This, however, is not enough to explain the frequencies in the upper stages. Predictions for $n = 1$ and infinity are also shown in figure 13. First, it is clear that the curve for $n = 1$ does not agree with any of the data. It is not clear why the 'fundamental tone' of the phenomenon is predicted with $n = 2$; one may speculate that the nozzle aspect ratio has an influence in determining this factor. Second, one notes that in the limiting case of an infinite number of vortices the first term in parentheses on the right-hand side of (3.1) becomes zero. This still predicts frequencies lower than the uppermost band in all cases, as illustrated by the curve for $n = \infty$ ('inf') in figure 13. In essence, the mechanism of the tones in the upper stages of figures 13–17 is not fully understood. It is not pursued further at the present time and in the following we examine the unsteady flow characteristics for a specific case of the resonance.

3.4. *Unsteady flow field under the resonance*

In this subsection data for plate *L*30 with $x_{TE} = 21.6$ and $z = -3.81$ at $Ma_j = 0.96$, yielding a tone at 1375 Hz, are discussed. Schlieren pictures of the flow field obtained at different phases within the tone period are obtained by using the microphone signal as a reference for triggering data acquisition. Such pictures at three phases are shown in figure 20 as examples. The axial motion of the unsteady flow structure with advancing phase can be seen clearly. At phase zero in figure 20(*a*), chosen arbitrarily,

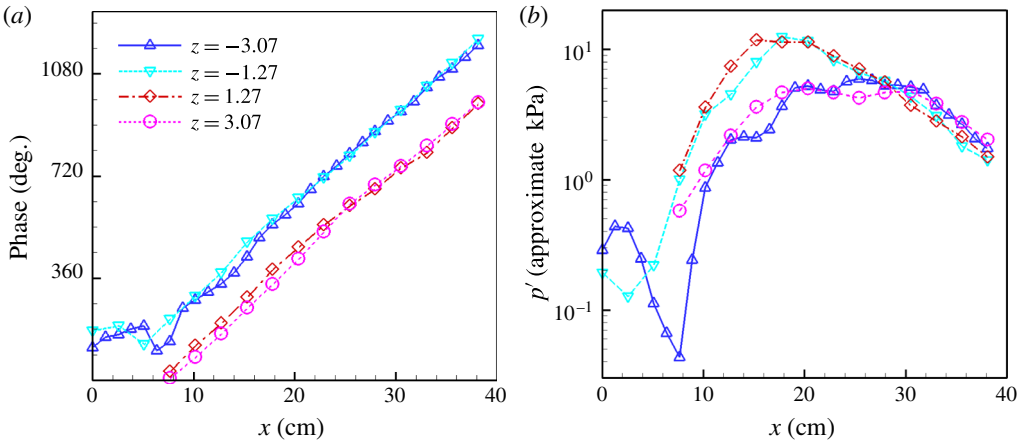

FIGURE 21. (Colour online) Streamwise variation of phase and amplitude of the tone fundamental; $L30$ plate at $x_{TE} = 21.6$, $z = -3.81$ producing tone at 1375 Hz. Data for four transverse (z) locations ($y = 0$). (a) Phase variation, (b) amplitude (r.m.s. of pressure fluctuation) variation. Data obtained by spectral analysis of signal from pressure transducer relative to microphone signal.

a trough in the unsteady flow structure is just leaving the trailing edge. One-third of the way into the period ($\varphi = 120°$ in figure 20b) a 'trough' occurs downstream of the TE. Two-thirds of the way ($\varphi = 240°$ in figure 20c), the trough is farther away while another trough upstream has approached the TE. The cycle then repeats itself.

Variations of the tone phase with streamwise distance, measured by the pressure transducer with the microphone signal as reference, are shown in figure 21(a). These data are taken at the centre span ($y = 0$) for four values of z, as indicated in the legend. For negative z-locations (closer to the plate) the data are obtained starting from the exit of the nozzle. For positive z-locations the data could not be obtained all the way to the nozzle exit due to hardware constraints. It can be seen that the phase variations for either the upper or the lower pair of traverses are similar but there is a consistent difference between the two pairs. Average phase velocities of $0.56U_j$ and $0.52U_j$ are estimated from the upper and lower pairs of curves, respectively.

Amplitude variations corresponding to the data of figure 21(a) are shown in figure 21(b). The transducer essentially sensed instantaneous total pressure. As stated in § 2, there was some uncertainty in the calibration and the absolute values of the amplitudes should be considered as qualitative. The amplitude data display the characteristics of an instability wave: initially growing, saturating to a peak and then decaying. The phase and amplitude variations in the transverse (z) direction, measured just downstream of the TE of the plate, are shown in figure 22. The phase variation exhibits a 180° jump across the centreplane of the jet. The amplitude drops at this location, grows and then decays in either direction of z. These data are consistent with a flapping motion of the jet column and the asymmetric vorticity distribution sketched in figure 18(a).

The schlieren pictures showed the structure of the flow field on the x–z cross-sectional plane. Phase-averaged flow field data were acquired to examine the corresponding unsteady characteristics on the cross-stream (y–z) plane. These data were acquired by traversing the pressure transducer on the y–z plane downstream of the plate's trailing edge ($x = 22.9$), for 19 phases within the period. Data for

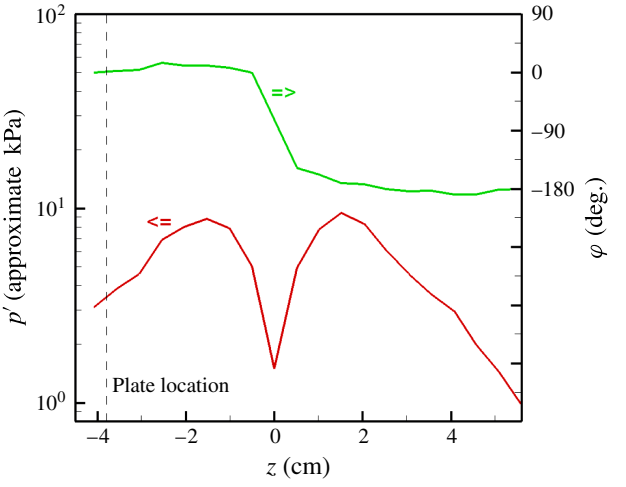

FIGURE 22. (Colour online) Phase and amplitude variation for the resonance case of figure 21 in the transverse (z) direction, downstream of the plate's trailing edge ($x = 22.9$, $y = 0$).

four phases are shown in figure 23(*b–e*), as examples. Corresponding time-averaged data are shown in figure 23(*a*). (The reference $\varphi = 0$ for these data and the pictures in figure 20 were assigned arbitrarily and there is no correspondence.) Estimated values of Mach number normalized by the jet Mach number Ma_j are plotted. The jet cross-section is seen to go through contortions and the unsteady motion is not simply an up-and-down flapping of the jet column against the plate.

The three-dimensional nature of the flow field is further illustrated by time-averaged Mach number contours measured at a far downstream location. These data, shown in figure 24 for the measurement location of $x = 64.5$ ($x/D = 12$) were acquired with standard Pitot probes. The distribution in figure 24(*a*) represents the same plate configuration as for figures 20–23 (plate $L30$ with $x_{TE} = 21.6$), yielding the resonant condition. It is clear that an axis switch has taken place. The major axis of the jet was horizontal at the exit of the nozzle but by the measurement station it has become vertical. Corresponding data with the plate drawn back are shown in figure 24(*b*). In this case there was no resonance and the data demonstrate that there was no axis switching. The jet cross-section gradually became round in this case with increase in x.

The data in figure 24(*a*) involve a resonance at $f_p \approx 1375$ Hz, corresponding to a Strouhal number ($f_p D/U_j$) of about 0.225, a value not too far from the 'preferred mode' for an equivalent axisymmetric jet. The resonance imposes a periodic forcing of the jet. Such forcing causes the rectangular jet to go through the axis switching due to the dynamics of the unsteady azimuthal vortical structures (Hussain & Husain 1989; Zaman 1996). A periodic forcing causes the sheet of azimuthal vorticity emanating from the nozzle to roll up into discrete vortex 'rings' (with initial shape determined by the geometry of the nozzle). The non-axisymmetric vortex rings go through self-induced contortions that lead to the axis switching. The key is the roll-up of the azimuthal vorticity into the non-axisymmetric rings. This may sometimes occur naturally, e.g. at low Reynolds numbers when the efflux boundary layer is laminar

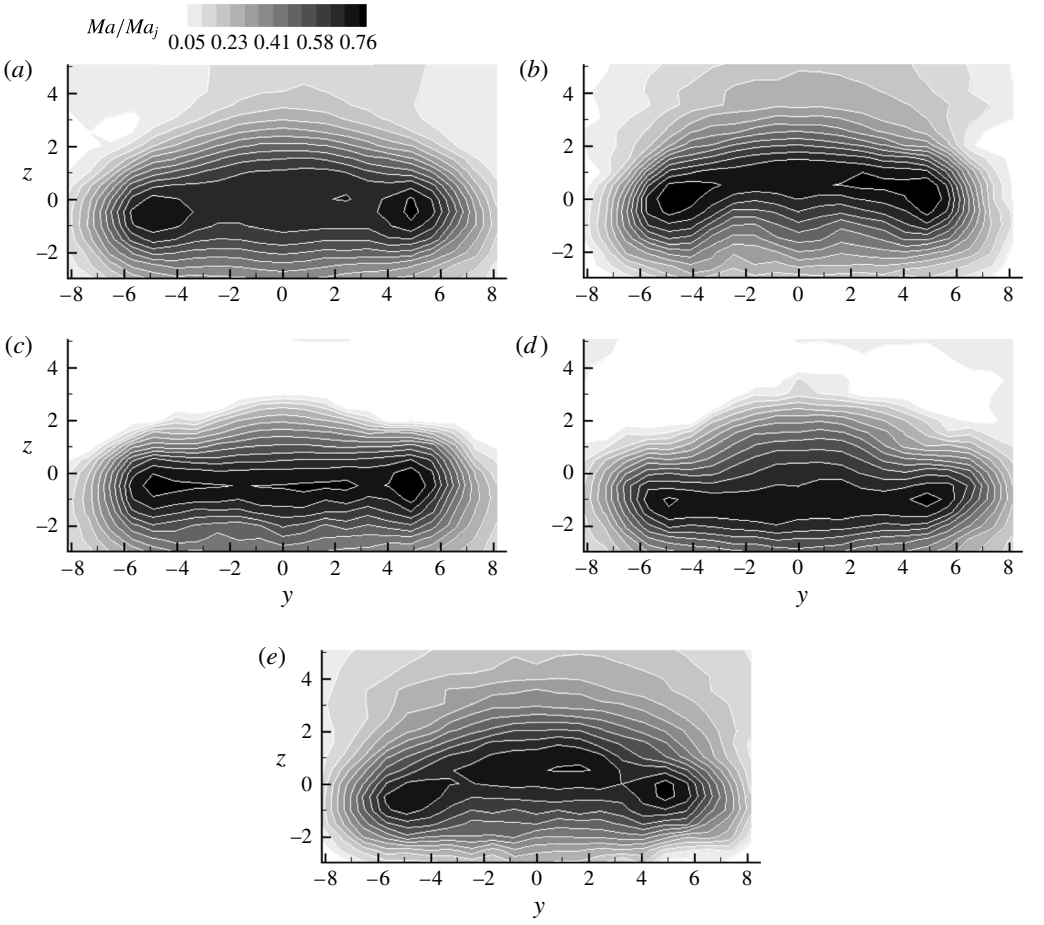

FIGURE 23. Cross-sectional distribution of Ma/Ma_j for plate $L30$ at $x = 22.9$ for the resonant condition of figures 20–22. Time-averaged data shown in (*a*); (*b–e*) show phase-averaged data at four phases: (*b*) $\varphi = 0°$; (*c*) $\varphi = 80°$; (*d*) $\varphi = 180°$ (*e*) $\varphi = 260°$. Coordinates are in cm.

and susceptible to naturally occurring disturbances. Periodic perturbations (e.g. by artificial excitation or naturally occurring phenomena such as screech), also yield the same effect. Without such periodic perturbation the axis switching is seldom observed at higher jet Reynolds number and Mach number, as is the case in figure 24(*b*). Thus, the axis switching is likely to be a result rather than the cause of the resonance in the present case. All resonant tones with the jet–surface configuration under study are expected to result in such axis switching as long as the frequency corresponds to a Strouhal number not too far from the value noted above.

The unsteady flow field data presented in this subsection illustrate the effect of the resonance on the flow field. Clearly, the assumption of two-dimensionality should be viewed with caution in any analysis of the flow. Furthermore, any numerical simulation must capture the unsteady effects, for otherwise calculation of even the mean flow field (e.g. captured in figure 24*a*) will not be possible.

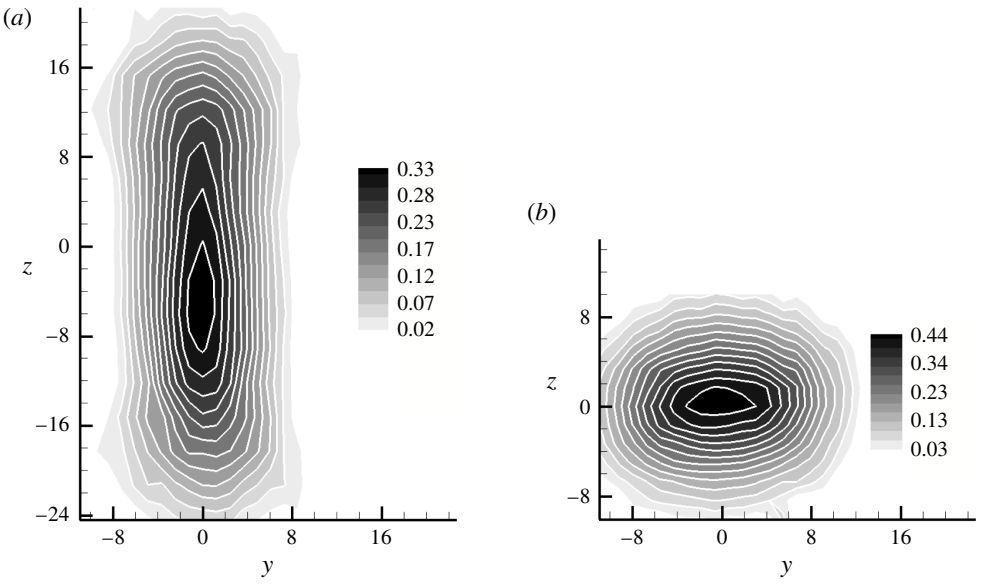

FIGURE 24. Time-averaged Ma/Ma_j contours at $x = 64.5$ for a resonant and a non-resonant condition with plate $L30$: (*a*) $x_{TE} = 21.6$, $z = -3.81$, $Ma_j = 0.96$ (resonance at 1375 Hz); (*b*) $x_{TE} = 7.6$, $z = -6.35$, $Ma_j = 0.96$ (plate drawn back, no resonance). Coordinates are in cm.

4. Conclusions

An experimental study has been conducted to investigate a resonance phenomenon occurring due to the interaction of a large aspect ratio rectangular jet with a flat plate. The plate is placed parallel to but away from the direct path of the jet. Care is taken to ensure that the resonance under consideration is not due to structural vibrations of the plate or the support mechanisms. The effect of parametric variation on the phenomenon is studied. For a given configuration, with increasing jet velocity the resonance is found to ensue at a high subsonic Mach number, become most prominent around the transonic condition and then stop abruptly at a low supersonic condition when shocks become prominent in the flow. It occurs for a range of transverse (z) positions of the plate relative to the jet. It disappears when the plate is either too far from or too close to the jet. With variation of the plate's z-location the frequency of the resonance varies only slightly. The frequency clearly increases with increasing jet Mach number and also for decreasing streamwise distance of the plate's trailing edge. It is noted that even when there is no audible tone, the noise spectra are marked by conspicuous peaks. It is demonstrated that for a fixed trailing edge location, the frequencies of the spectral peaks also depend on the location of the leading edge. An acoustic feedback is considered and shown to explain the 'fundamental' tone frequency. However, this does not explain all the peaks and the full mechanism of the phenomenon is still not completely clear. Under the resonant condition the jet cross-section goes through an 'axis-switching' and flow visualization indicates a periodic flapping motion of the jet column. The details of the unsteady characteristics of the flow field for a specific case of the resonance are documented.

Acknowledgements

Thanks are due to Ms M. Clem for help with schlieren flow visualization and to Drs S. Leib and B. Henderson for helpful inputs. Support from the Commercial Supersonic Technology (CST) and Advanced Air Transport Technology (AATT) Projects of NASA's Advanced Air Vehicles Program is gratefully acknowledged.

REFERENCES

AFSAR, M., GOLDSTEIN, M. E. & LEIB, S. J. 2013 Prediction of low-frequency trailing edge noise using rapid distortion theory. In *14th European Turbulence Conference, Ecole Normale Superieure de Lyon, Lyon, France*.

BALSA, T. F., GLIEBE, R. R., KANTOLA, R. A., MANI, R. & STRINGAS, E. J. 1978 High velocity jet noise source location and reduction, Task 2 – theoretical developments and basic experiments. *Report No.* R78AEG323, FAA-RD-76-79-2, General Electric Co., Aircraft Engine Group, Cincinnati, OH.

BRIDGES, J. E., BROWN, C. A. & BOZAK, R. F. 2014 Experiments on exhaust noise of highly integrated propulsion systems. *AIAA Paper* 2014-2904, *21st AIAA/CEAS Aeroacoustics Conference, Atlanta, GA*.

BROWN, W. H. & AHUJA, K. K. 1984 Jet and wing/flap interaction noise. *AIAA Paper* 84-2362, *9th AIAA Aeroacoustics Meeting, Williamsburg, VA*.

BROWN, C. A. & WERNET, M. P. 2014 Jet surface interaction test: flow measurements results. *AIAA Paper* 2014-3198, *21st AIAA/CEAS Aeroacoustics Conference, Atlanta, GA*.

BROWN, G. B. 1937 The vortex motion causing edge tones. *Proc. Phys. Soc. Lond.* **49**, 493–507.

CRIGHTON, D. 1991 Airframe noise. In *Aeroacoustics of Flight Vehicles: Theory and Practice, Volume 1: Noise Sources* (ed. H. H. Hubbard), NASA Reference Publication 1258, vol. 1, chap. 7.

FAGAN, A. F., L'ESPERANCE, D. & ZAMAN, K. B. M. Q. 2014 Application of a novel projection focusing schlieren system in NASA test facilities. *AIAA Paper* 2014-2522, *31st AIAA Aerodynamic Measurement Technology and Ground Testing Conference, Atlanta, GA*.

FRATE, F. C. & BRIDGES, J. E. 2011 Extensible rectangular nozzle model system. *AIAA Paper* 2011-975, *49th Aerospace Sciences Meeting, Orlando, FL*.

GOLDSTEIN, M. E., AFSAR, M. Z. & LEIB, S. J. 2013 Non-homogeneous rapid distortion theory on transversely sheared mean flows. *J. Fluid Mech.* **736**, 532–569.

HUSSAIN, F. & HUSAIN, H. S. 1989 Elliptic jets. Part 1. Characteristics of unexcited and excited jets. *J. Fluid Mech.* **208**, 257–320.

JONES, R. R. & LAZALIER, G. R. 1992 The acoustic response of altitude test facility exhaust systems to axisymmetric and two-dimensional turbine engine exhaust plumes. *Paper* 92-02-131, *DGLR/AIAA Aeroacoustics Conference, Aachen, Germany*.

MASSEY, K. C., AHUJA, K. K. & GAETA, R. 2004 Noise scaling for unheated low aspect ratio rectangular jets. *AIAA Paper* 2004-2946, *10th AIAA/CEAS Aeroacoustics Conference, Manchester, UK*.

MEAD, C. J. & STRANGE, P. J. R. 1998 Under-Wing Installation effects on Jet Noise at Sideline. *AIAA Paper* 98-2207, *4th AIAA/CEAS Aeroacoustics Conference, Toulouse, France*.

MENGLE, V. G. 2011 The effect of nozzle-to-wing gulley height on jet flow attachment to the wing and jet-flap interaction noise. *AIAA Paper* 2011-2705, *17th AIAA/CEAS Aeroacoustics Conference, Portland, Oregon*.

MILLER, W. R. 1983 Flight effects for jet–airframe interaction noise. *AIAA Paper*-83-0784, *8th AIAA Aeroacoustics Conference, Atlanta, Georgia*.

NICHOLS, J. W., HAM, F. E., LELE, S. K. & MOIN, P. 2011 Prediction of supersonic jet noise from complex nozzles. In *Center for Turbulence Research, Stanford University, Annual Research Briefs*, pp. 3–14.

NOMOTO, H. & CULICK, F. E. C. 1982 An experimental investigation of pure tone generation by vortex shedding in a duct. *J. Sound Vib.* **84** (2), 247–252.

OLSEN, W. & BOLDMAN, D. 1979 Trailing edge noise data with comparison to theory. *AIAA Paper* 79-1524, *12th Fluid and Plasma Dynamics Conference, Williamsburg, VA*.

POWELL, A. 1953 On the mechanism of choked jet noise. *Proc. Phys. Soc. Lond.* B **66**, 1039–1056.

POWELL, A. 1961 On the edgetone. *J. Acoust. Soc. Am.* **33**, 395–409.

ROCKWELL, D. & NAUDASCHER, E. 1979 Self-sustained oscillations of impinging shear layers. *Annu. Rev. Fluid Mech.* **11**, 67–93.

SENGUPTA, G. 1983 Analysis of jet–airframe interaction noise. *AIAA Paper* 83-0783, *8th Aeroacoustics Conference, Atlanta, Georgia*.

TAM, C. K. W. & YU, J. C. 1975 Trailing edge noise. *AIAA Paper* 75-489, *2nd Aeroacoustics Conference, Hampton, VA*.

TAM, C. K. W. 1995 Supersonic jet noise. *Annu. Rev. Fluid Mech.* **27**, 17–43.

SAMANTA, A. & FREUND, J. B. 2008 Finite-wavelength scattering of incident vorticity and acoustic waves at a shrouded-jet exit. *J. Fluid Mech.* **612**, 407–438.

VON GLAHN, U. H. 1989 Rectangular nozzle plume velocity modeling for use in jet noise prediction. *AIAA Paper* 89-2357, *25th Joint Propulsion Conference, Monterey, CA*.

WAY, D. J. & TURNER, B. A. 1980 Model tests demonstrating under-wing installation effects on engine exhaust noise. *AIAA Paper* 80-1048, *6th Aeroacoustics Conference, Hartford, CT*.

YU, J. C. & TAM, C. K. W. 1978 Experimental investigation of trailing edge noise mechanism. *AIAA J.* **16** (10), 1046–1052.

ZAMAN, K. B. M. Q. 1996 Axis switching and spreading of an asymmetric jet: the role of coherent structure dynamics. *J. Fluid Mech.* **316**, 1–27.

ZAMAN, K. B. M. Q. 2012 Flow-field surveys for rectangular nozzles. *NASA Tech. Rep.* TM-2012-217410 (also *AIAA Paper* 2012-0069).

ZAMAN, K. B. M. Q., CLEM, M. M. & FAGAN, A. F. 2013 Noise from a jet discharged into a duct and its suppression. *Intl J. Aeroacoust.* **12** (3), 189–214.

ZAMAN, K. B. M. Q., FAGAN, A. F., CLEM, M. M. & BROWN, C. A. 2014 Resonant interaction of a rectangular jet with a flat-plate. *AIAA Paper* 2014-2522, *52nd Aerospace Sciences Meeting, SciTech-2014, National Harbor, MD*.